



## JWST TECHNICAL REPORT

Title: Quantification of charge migration in NIRISS Aperture Masking Interferometry data.	Doc #: JWST-STScI-009185, SM-12 Date: 12 November 2025 Rev: -
Authors: Deepashri Thatte & Paul Goudfrooij Phone: x4462	Release Date: 17 November 2025

### 1 Abstract

Charge migration was observed in Teledyne HAWAII-2RG detectors used in the NIRCam, NIRISS, and NIRSpec science instruments aboard the James Webb Space Telescope (JWST). The charge migration takes place when new photoelectrons in a given pixel are repelled by previously accumulated photoelectrons causing them to migrate to adjacent pixels that have lower charge. This results in a non-linear detector response called brighter-fatter effect (BFE) in which a brighter source produces a larger image than a fainter source blurring the intensity distribution of brighter sources more than it does for fainter sources. We quantify the signal levels at which this charge migration causes the count rate of the peak pixel drop by 1% for NIRISS Aperture Masking Interferometry (AMI) data, while count rate in 3x3 and 5x5 pixel windows remains linear. This signal level is the `signal_threshold` parameter used by the `charge_migration` step of the JWST Detector 1 pipeline. Groups whose signal level exceeds the `signal_threshold` value are not included in ramp slope calculations. The JWST Exposure Time Calculator uses it as a signal limit to determine maximum number of groups before “saturation” (even though that limit is lower than that of physical saturation). We find `signal_threshold` values of 14465 ADU, 14220 ADU, 13883 ADU and 13290 ADU respectively for the four filters F480M, F430M, F380M and F277W with the non-redundant mask (NRM) of the AMI mode in place.

### 2 Introduction

NIRISS AMI mode enables high-contrast, high-resolution imaging of sources around bright stars, and is designed to detect point sources that are separated by  $\sim 75 - 500$  mas with a brightness ratio as small as  $10^{-4}$  (Sivaramakrishnan et al. 2023). It uses a non-redundant aperture mask (NRM) in the pupil wheel with one of three medium-band filters (F380M, F430M, and F480M) or a wide-band filter (F277W) in the filter wheel. The 7-hole mask turns the full aperture of the telescope into an interferometric array, generating an interferogram in the image plane. AMI data reduction involves

reducing these interferometric data to fringe observables of closure phases (CP) and square visibility (SqV). These observables enable measurement of binary point source parameters such as contrast, separation and position angle and are used in image reconstruction of extended sources. An understanding of the effects of charge migration and its mitigation on the extraction of observables is therefore crucial.

Sallum et al. (2024) used self-calibration tests to show that signal-dependent changes due to charge migration cause contrast degradation and that charge migration is the dominant source of scatter in the calibrated closure phases of the source. The non-linearity introduced by charge migration is not straightforward to correct in the Fourier space. A joint implementation of a differentiable physics model of the optics, and a machine-learned Effective Detector Model (EDM) called dLux was introduced by Desdoigts, Pope, & Tuthill (2024). Their preliminary calibrations have shown these to be effective in modeling the non-linear effects.

Goudfrooij et al. (2024) describe the effects of BFE on NIRISS imaging data and introduce an algorithm that mitigates the effects of charge migration. This algorithm was (implemented as a new step in the `calwebb_detector1` pipeline in between the `dark_current` and `jump` steps in JWST Science Calibration Pipeline version 1.12.0 to 1.12.5 that was released with Build 10.0.2. on 12/05/2023. This step takes `signal_threshold` as an input parameter above which pixels get a data quality (DQ) flag entitled CHARGELOSS. The groups with this flag are excluded from ramp slope calculations. They are however not issued a jump flag and thus included in the calculation of the variance of the slope due to read noise. The goal of the analysis presented here is to quantify the `signal_threshold` value for NIRISS AMI data observed with filters F480M, F430M, F380M and F277W.

### 3 Observations

We looked at and did preliminary analysis of several available NIRISS datasets to find data suitable for quantifying the `signal_threshold`. NIRISS AMI calibration programs CAL-NIS-017 (PID 1509, Cycle 1) and CAL-NIS-216 (PID 4481, Cycle 2) were identified for quantifying `signal_threshold` for three medium band filters F480M, F430M and F380M used with the AMI mode. Program 1509 includes F480M observations of HR 7258 at dither position POS1, having 45 integrations with 115 groups in each integration. The long length of the ramp combined with 2MASS  $K_s$  magnitude 6.872, reaching  $\sim 39,000$  ADU in the peak pixel in last group of the ramp, makes this dataset an ideal candidate to understand the behavior of charge migration. It has enough groups up the ramp for reliable ramp slope measurement, and to observe the evolution of charge migration as the ramp accumulates more charge. The star is bright enough to be able to observe a 1% drop in slope for quantifying threshold and observe further decrease in slope over the length of the ramp. This drop would have been hard to quantify for a significantly brighter star, since it would require fewer groups for the peak pixel to reach a similar signal level, thus leaving fewer data points to measure precise ramp slopes. (Conversely, this drop would have also been hard to observe for a fainter star with equivalent ramp length since it would require more groups for the peak pixel to reach a similar signal level and additional groups to observe 1% drop in slope.) However, the program 1509 observation only used the F480M filter. We will use the results from this dataset to scale the `signal_threshold` values calculated from program 4481 data which has fewer groups per integration (e.g. NGROUPS = 30 for F480M observation), but for all AMI

Check with the JWST SOCCER Database at: <https://soccer.stsci.edu>  
To verify that this is the current version.

medium-band filters. It includes 3 medium band filter (F480M, F430M, F380M) observations of HD 41094 with WISE W2 magnitude 6.006 (2MASS  $K_s$  magnitude 6.022) at dither position POS1. We then use these scaling factors to calculate `signal_threshold` for F430M and F380M data from program 4481.

Table 1 shows relevant information about the exposures used in this analysis.

**Table 1: Calibration program 1509 and 4481 exposure information**

Filename	Target	Brightness 2MASS $K_s$	Pupil Filter	Subarray	NGROUPS	NINTS
jw01509003001_05101_00001_nis_ramp.fits	HR 7258	6.872± 0.023	NRM F480M	SUB80	115	45
jw01509003001_07101_00001_nis_ramp.fits	HR 7258	6.872± 0.023	NRM F480M	SUB80	115	45
jw04481001001_03102_00001_nis_ramp.fits	HD 41094	6.022± 0.024	NRM F480M	SUB80	30	760
jw04481001001_03104_00001_nis_ramp.fits	HD 41094	6.022± 0.024	NRM F380M	SUB80	11	1060
jw04481001001_03106_00001_nis_ramp.fits	HD 41094	6.022± 0.024	NRM F430M	SUB80	20	905

## 4 Calibration and Analysis

The data were calibrated using JWST Detector 1 pipeline (Bushouse et al. 2024) version 1.18.1, with the `charge_migration` step turned off. A linearity correction step that corrects the pixel values for detector non-linearity was applied. This step depends on charge in a pixel, but not on charge in the neighboring pixels. Figure 1 shows the last group of the ramp for program 1509 and program 4481 data at dither position POS1. There are two exposures of HR 7258 at dither position POS1. We will identify these exposures as POS1a and POS1b throughout this document. Charge migration is most significant when the contrast between neighboring pixels is the highest (Hirata & Choi 2020). If the centroid of the PSF is near the center of a pixel, the contrast with neighboring pixels is higher compared to when the centroid is near the pixel corner or edge. We therefore looked at the PSF centroids for both POS1 exposures of HR 7258 and identified POS1b as slightly more symmetric; hence this exposure was used to quantify the charge migration threshold for F480M. For program 4481, only one exposure in each filter was available at POS1.

The 9 individual pixels centered around the peak (see Figure 2) and the sum of the inner 3x3 and 5x5 pixels from the ramp.fits files were used for the analysis. We will refer to the individual pixels and the sums as 11 separate “pixel types” in rest of the document.

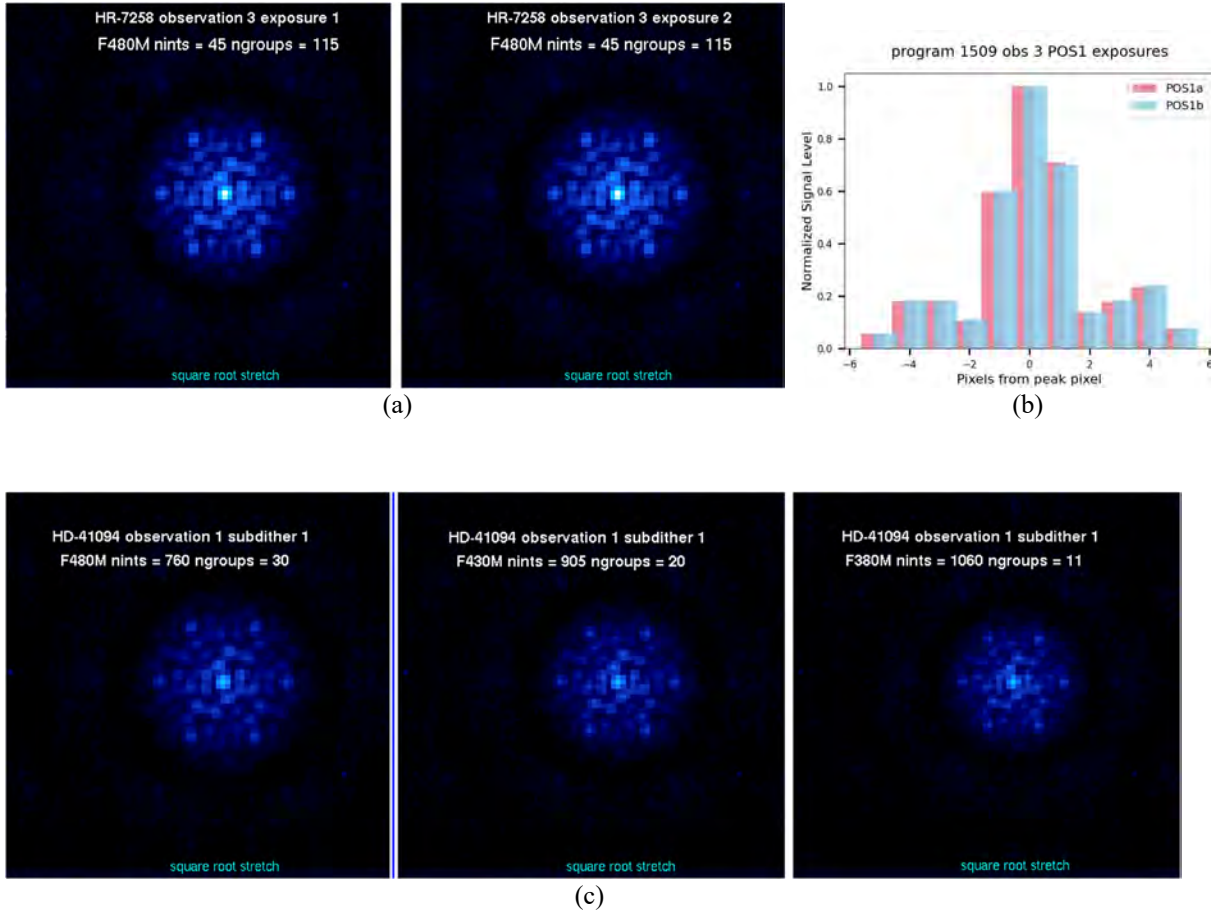


Figure 1. NIRISS AMI Calibration program 1509 observations of HR 7258. Panel (a) shows the last group of the ramp for NRM and F480M exposures at dither position POS1 (POS1a and POS1b). Panel (b) shows the centroid of the PSF of the exposures from panel (a) where POS1b exposure is slightly more symmetric compared to POS1a exposure. Panel (c) shows calibration program 4481 data of HD 41094 at dither position POS1 for filters F480M, F430M and F380M. POS1 data from both programs were used for quantifying signal\_threshold. The data are displayed on a square root stretch with matching scale.



Figure 2. Central 9-pixel region used for analysis. Nine pixel types p (peak), E, W, N, S, NE, SE, SW and NW are marked.

Figure 3 shows mean counts in a group across all integrations as a function of NGROUPS for the F480M exposure in program 1509. The peak pixel and the second brightest pixel clearly show a deviation from linearity with increasing NGROUPS. Some neighboring pixels with lower signal levels appear to have *gained* charge. This is the charge that has migrated from the bright pixels to the neighboring pixels. However, the sum of 3x3 and 5x5 pixels around the peak pixel stays linear with NGROUPS as seen in panel (b). In other words, the total accumulated charge in the PSF is not affected by charge migration (see also Goudfrooij et al. 2024).

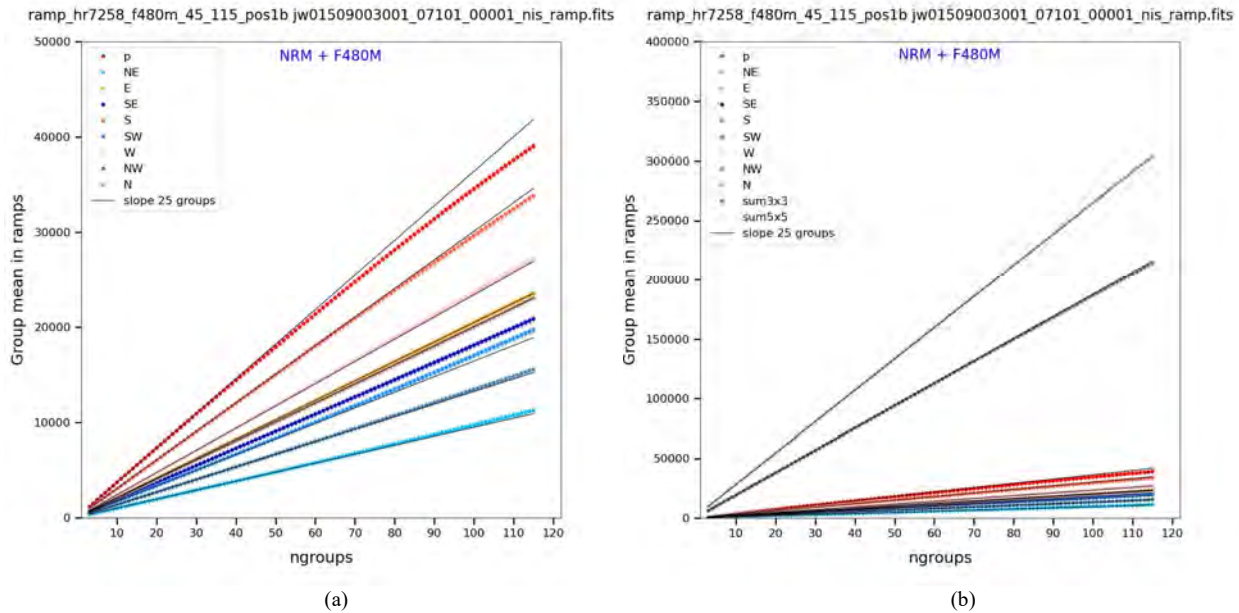


Figure 3. Group mean across all integrations in program 1509 F480M POS1 ramp file for (a) 9 pixel types p (peak), E, W, N, S, NE, SE, SW and NW and (b) sums of inner 3x3 and 5x5 pixels.

Calibration program 4481 observations of HD 41094 reach  $\sim 23000$  ADUs in the peak pixel in F480M, F430M and F380M observations. Figure 4 shows mean counts in the groups across integrations for 11 pixel types in these observations.

For both datasets we calculate weighted averaged ramp slopes and weighted averaged slope error for groups N with  $3 \leq N \leq \text{NGROUPS}$  across all integrations in the rampfile for the 11 pixel types. For example, program 1509 data have two exposures at dither position 1 with  $\text{ngroups} = 115$  and  $\text{nints} = 45$ . For the 11 pixel types in this dataset we calculate “baseline” slopes for the first 3 groups, first 4 groups and so on until group 115. The reason for choosing a minimum of 3 groups is to calculate covariance. We then define the “fractional count rate” similar to Goudfrooij et al. (2024):

$$\text{fracrate}_{\text{NG}} = \text{slope}_{\text{NG}} / \text{slope}_{\text{baseline\_NG}}.$$

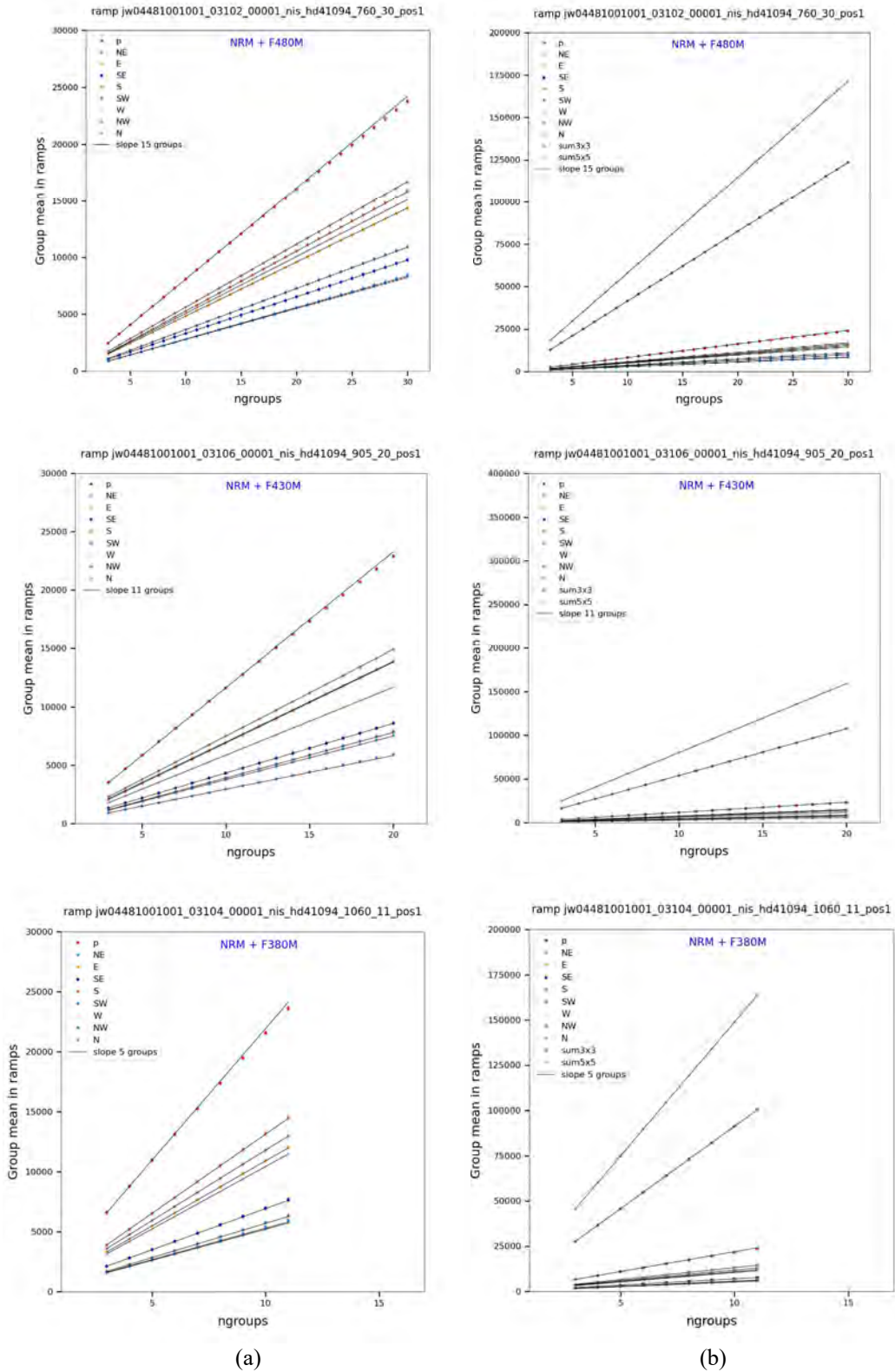
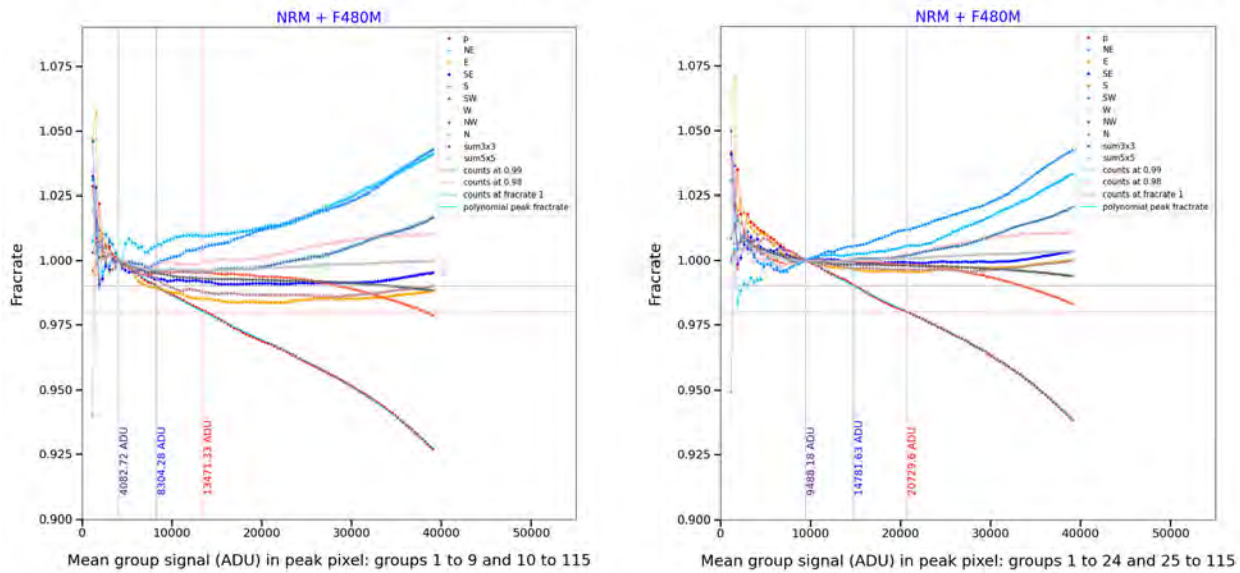


Figure 4. Group mean across all integrations in program 4481 F480M POS1 ramp file. Column (a) 9 individual pixel types and column (b) sum of inner 3x3 and 5x5 pixels. The top row shows F480M data, the middle row shows F430M data and the bottom row shows F380M data.

Check with the JWST SOCCER Database at: <https://soccer.stsci.edu>  
 To verify that this is the current version.

We study the behavior of the *fracrate* curve for a range of baseline number of groups used for calculating slope<sub>baseline\_NG</sub>. Figure 5 shows fractional count rate as a function of mean counts in all ramps for three of the many baseline number of groups values that we looked at. We use the *fracrate* for baseline groups to be able to see the evolution of fracrate before and after a baseline group and see where it starts showing a similar trend in fracrate or where the behavior stabilizes. We then look at the baseline group for which the counts in the peak pixel are  $\approx 9,000$  ADU (to get a good enough SNR), while the shape of the *fracrate* curve for the peak pixel decreases consistently after that baseline group, as expected from charge migration. We identify the signal levels at which

Fracrate for base slope with 10 groups pdeg 3 ramp\_hr7258\_f480m\_45\_115\_pos1b    Fracrate for base slope with 25 groups pdeg 3 ramp\_hr7258\_f480m\_45\_115\_pos1b



Fracrate for base slope with 35 groups pdeg 3 ramp\_hr7258\_f480m\_45\_115\_pos1b

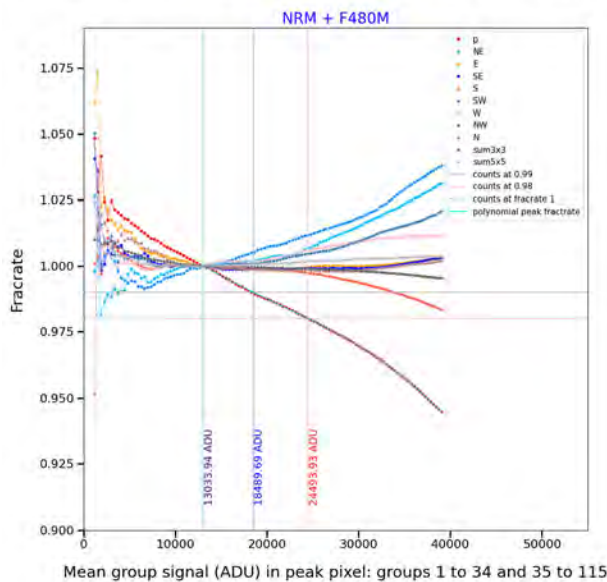


Figure 5. Fractional count rate as a function of mean counts in 11 pixel types for HR 7258 F480M data with nints = 45 and ngroups = 115 for three different baseline ngroup values of 10, 25 and 35.

Check with the JWST SOCCER Database at: <https://soccer.stsci.edu>  
To verify that this is the current version.

*fracrate* equals 0.99 of the peak pixel *fracrate*, i.e., the signal levels at which charge migration has caused the count rate to decrease by 1%. For program 1509 data, we identify group 25 as the baseline group. (The linear fit shown Figure 3 also uses the same baseline group of 25.) We apply least squares polynomial fits to the *fracrate* and peak pixel counts from the baseline group and higher. The 1% drop in *fracrate* calculated by evaluating the roots of the polynomial is at 14781.63 ADU. We use the polynomial to calculate the 1% drop in peak pixel count rate if the peak pixel counts were 9500 ADU. The reason for choosing 9500 ADU is to use a uniform peak pixel value for POS1a and POS1b data. The value corresponding to the 1% drop is 14465.18 ADU which we identify as *signal\_threshold* for F480M. This value is slightly lower than 14781.63 ADUs seen in panel (b) of Figure 5. This is due to the small deviation of fitted *fracrate* from measured *fracrate* (see figure 6).

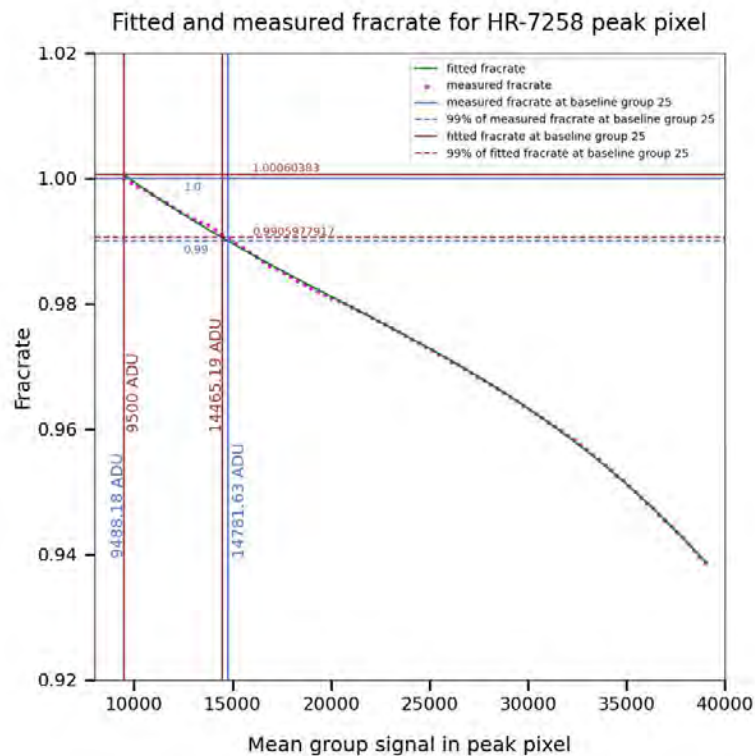
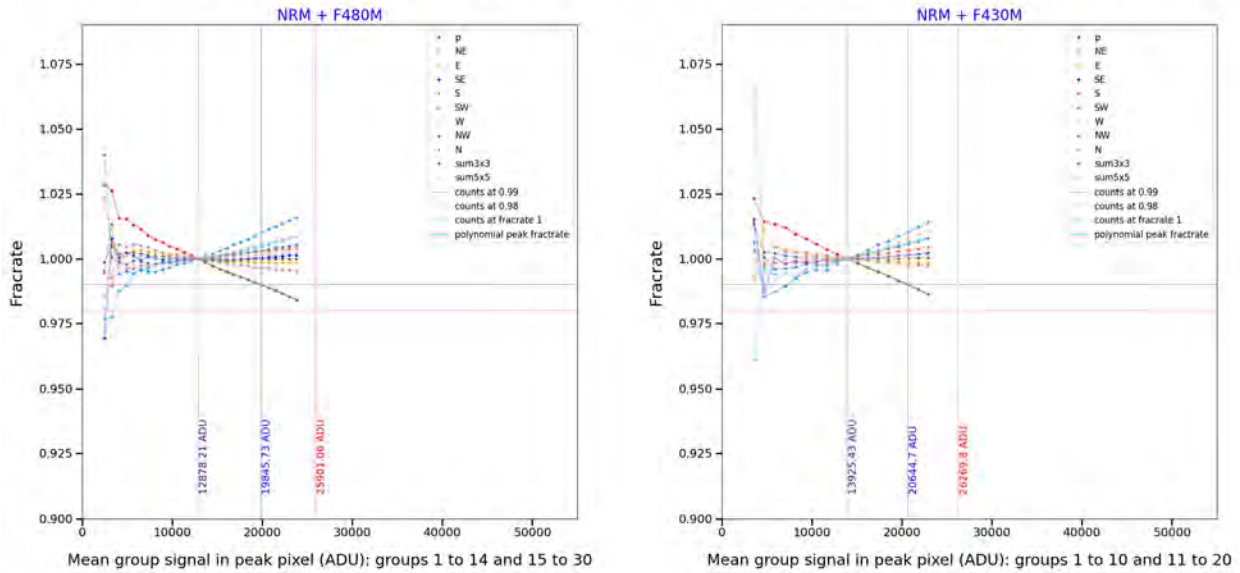


Figure 6. Measured and fitted *fracrate* corresponding to baseline group of 25. Mean counts 14465.19 ADU is the *signal\_threshold* for NRM+F480M data of HR 7258.

We use the F480M *signal\_threshold* of 14465.18 ADU as a reference signal and use it to scale the *signal\_threshold* calculated from program 4481 F480M data that has fewer groups (*ngroups* = 30), and thus lower measurement precision, compared to 115 groups from program 1509. We then use this scaling factor and the F480M reference signal threshold to calculate *signal\_threshold* for filters F430M and F380M. Figure 7 shows the fractional count rate plots with identified baseline groups for F480M, F430M and F380M data from program 4481.

Fracrate for base slope with 15 groups pdeg 3 ramp\_hd41094\_f430m\_905\_20\_pos1    Fracrate for base slope with 11 groups pdeg 3 ramp\_hd41094\_f430m\_905\_20\_pos1



Fracrate for base slope with 5 groups pdeg 3 ramp\_hd41094\_f430m\_905\_20\_pos1

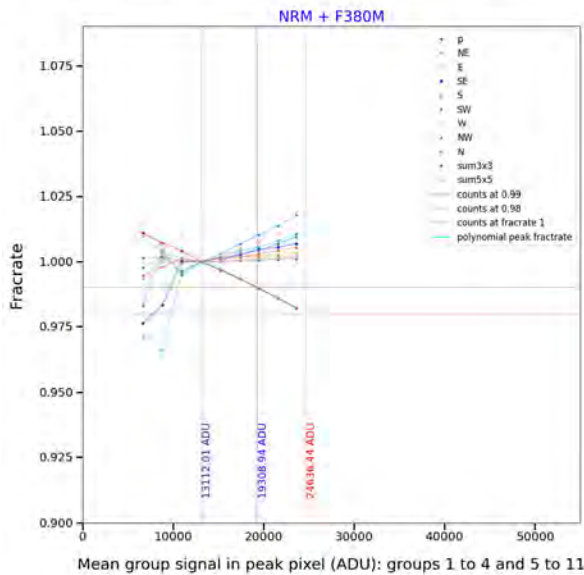


Figure 7. Fractional count rate as a function of mean counts in 11 pixel types for HD 41094 data for F480M, F430M, F380M. The baseline groups for each filter are identified in the figure.

We identify 13000 ADUs as baseline counts for HD 41094 peak pixel POS1 data for F480M, F430M, and F380M and calculate signal threshold corresponding to 1% drop in peak pixel counts of 13000 ADU. These values are 20036.70 ADU, 19697.42 ADU and 19229.87 respectively. We then calculate a scaling factor  $19697.42/20036.70$  between F430M signal threshold and F480M signal threshold corresponding to these baseline counts. Similarly, we calculate a scaling factor  $19229.87/20036.70$  for F380M. We multiply these scaling factors by the reference F480M signal threshold of 14465.18 ADU (which was derived from program 1509) to get final signal threshold values for F430M and F380M. These are listed in Table 2.

Check with the JWST SOCCER Database at: <https://soccer.stsci.edu>

To verify that this is the current version.

Table 2. Signal threshold at which charge migration has caused the ramp slope to decrease by 1%. The “reference” signal threshold of 14465.18 ADU measured from program 1509 F480M data with ngroups = 115 and the F480M threshold measured from program 4481 F480M data with ngroups = 30 were used to scale F430M and F380M data to calculate `signal_threshold` for those filters.

Program 4481 POS1 data	Filter	ngroups	nints	Peak pixel signal threshold for baseline counts of 13000 ADU <code>S_0.99_13000_filter</code>	R_filter = <code>S_0.99_13000_filter/</code> <code>S_0.99_13000_F480M</code>		Signal_threshold (ADU)  <code>R_filter * F480M_ref</code> ( <code>F480M_ref = 14465.18</code> ADU)	
jw04481001001_03102_00001_nis_ramp.fits	F480M	30	760	20036.69	R_480M	20036.70/ 20036.70	R_480M * 14465.18	14465.18
jw04481001001_03106_00001_nis_ramp.fits	F430M	20	905	19697.42	R_430M	19697.42/ 20036.70	R_F430M * 14465.18	14220.25
jw04481001001_03104_00001_nis_ramp.fits	F380M	11	1060	19229.87	R_380M	19229.87/ 20036.70	R_F380M * 14465.18	13882.71

As discussed in Goudfrooij et al. (2024), charge migration depends on filter wavelength due to increasing pixel to pixel contrast as the PSF gets narrower with decreasing wavelength.

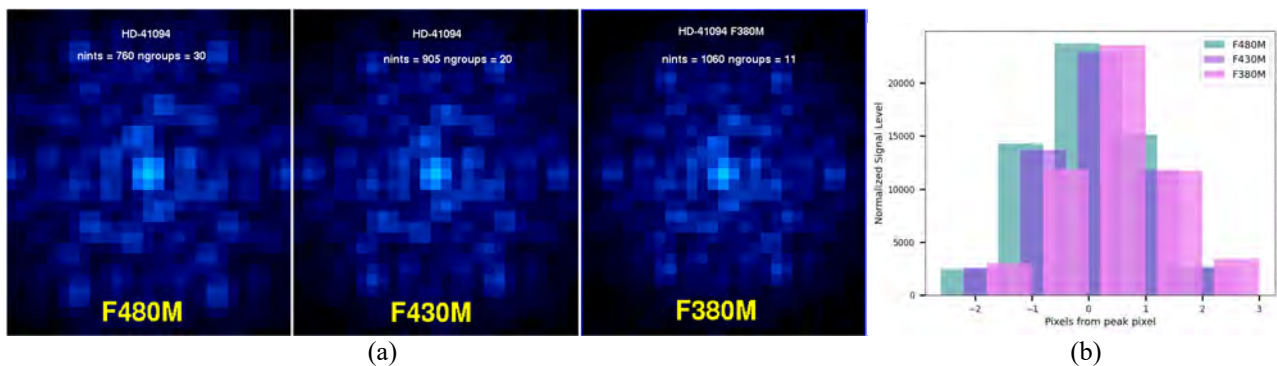


Figure 8. F480M, F430M, F380M PSFs from program 4481. Note that (a) PSFs get narrower and (b) contrast between neighboring pixels decreases with increasing wavelength.

Figure 8 shows last group of the ramp in a single integration for NRM + Filter PSFs for three medium-band AMI filters F480M, F430M and F380M. The PSF gets narrower and the contrast of the peak pixels with neighboring pixels increases from F480M → F430M → F380M.

The NIRISS AMI mode also supports observations with the wide-band filter F277W. However, data suitable for quantification of the charge migration threshold were not available. We therefore did a linear extrapolation of medium-band `signal_threshold` values shown in Table 2 with filter central wavelength to estimate the signal threshold for F277W. This results in a signal

Check with the JWST SOCCER Database at: <https://soccer.stsci.edu>  
To verify that this is the current version.

threshold value of 13289.77 ADU for F277W.

## 5 Results

Figure 9 and Table 3 show the results of our analysis to quantify `signal_threshold` for the 4 NIRISS filters F480M, F430M, F380M and F277W.

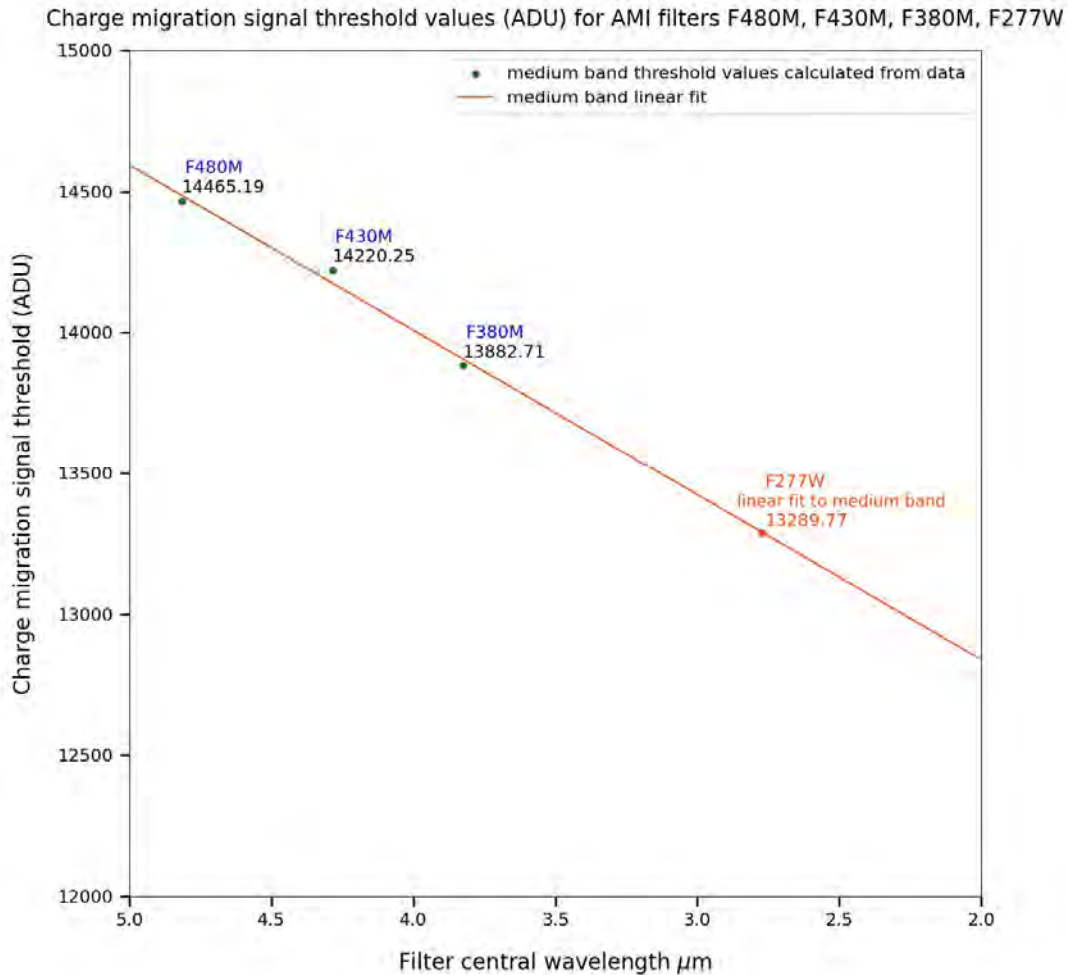


Figure 9. Charge migration signal threshold values for NIRISS AMI filters F480M, F430M, F380M, and F277W. The medium-band values were calculated using POS1 data of HR 7258 and HD 41094 respectively from programs 1509 and 4481. Signal threshold for F277W was estimated using linear extrapolation of medium-band signal threshold values as explained in the text.

Table 3. Charge migration `signal_threshold` values for NIRISS AMI filters

NRM + Filter	Signal threshold ADU
F480M	14465.19
F430M	14220.25
F380M	13882.71
F277W	13289.77

## 6 Conclusions

NIRISS AMI data are affected by brightness-dependent changes in PSF morphology, caused by a non-linear response of the detector called the “brighter-fatter effect” (BFE). This is a physical effect where photoelectrons migrate from a pixel with high charge into neighboring pixels with lower charge as they are repelled by previously accumulated photoelectrons. We analyze existing data from NIRISS AMI cycle 1 and cycle 2 calibration programs to quantify charge migration. The relevant parameter is called `signal_threshold` and it is a signal level at which charge migration causes the count rate of the peak pixel to drop by 1%. F480M observations of HR 7258 with 115 groups and 45 integrations were used to quantify the reference `signal_threshold` for the F480M filter. This `signal_threshold` was used with F480M, F430M and F380M data with fewer ngroups (30, 20, 11 respectively for the three filters) from program 4481 to calculate signal threshold values for filters F430M and F380M. Finally, the F277W signal threshold was calculated using linear extrapolation of the medium-band signal threshold values. These values are now used by the `charge_migration` step of the JWST Detector 1 pipeline to mitigate the effects of charge migration for AMI data. The `signal_threshold` parameter values in the parameter reference files were updated with these values and the updated files `jwst_niriss_pars-chargemigrationstep_0041.asdf` (F277W), `jwst_niriss_pars-chargemigrationstep_0040.asdf` (F380M), `jwst_niriss_pars-chargemigrationstep_0039.asdf` (F430M), and `jwst_niriss_pars-chargemigrationstep_0038.asdf` (F480M) were delivered to the JWST Calibration Reference Data System (CRDS) on June 17, 2025.

The signal threshold level is also used by the JWST ETC via the `niriss.json` file to determine the exposure parameters. These values are listed under ‘fullwell’ in units of electrons in the `niriss.json` file. This full-well value is the signal limit that is used to determine maximum number of groups before saturation to enable mitigation of charge migration and is lower than the true non-linearity based saturation limit. We converted the `signal_threshold` values in ADU to electrons by multiplying it by a gain of 1.61 e-/ADU.

## 7. References

Bushouse, H., Eisenhamer, J., Dencheva, N., Davies, J., Greenfield, P., Morrison, J., Hodge, P., Simon, B., Grumm, D., Droettboom, M., Slavich, E., Sosey, M., Pauly, T., Miller, T., Jedrzejewski, R., Hack, W., Davis, D., Crawford, S., Law, D., Gordon, K., Regan, M., Cara, M., MacDonald, K., Bradley, L., Shanahan, C., Jamieson, W., Teodoro, M., Williams, T., & Pena-Guerrero, M. (2024). JWST Calibration Pipeline (Version 1.18.1) [Computer software]. <https://doi.org/10.5281/zenodo.7038885>

Check with the JWST SOCCER Database at: <https://soccer.stsci.edu>

To verify that this is the current version.

Paul Goudfrooij, David Grumm, Kevin Volk, and Howard Bushouse; An Algorithm to Mitigate Charge Migration Effects in Data from the Near Infrared Imager and Slitless Spectrograph on the James Webb Space Telescope 2024 *PASP* **136** 014503 [DOI 10.1088/1538-3873/ad1c98](https://doi.org/10.1088/1538-3873/ad1c98)

Louis Desdoigts, Benjamin Pope, and Peter Tuthill, Differentiable modelling and data analysis for the JWST aperture masking interferometer," *Proc. SPIE* 13095, Optical and Infrared Interferometry and Imaging IX, 1309513 (28 August 2024); <https://doi.org/10.1117/12.3020303>

Steph Sallum *et al* 2024 The JWST Early Release Science Program for Direct Observations of Exoplanetary Systems. IV. NIRISS Aperture Masking Interferometry Performance and Lessons Learned, *ApJL* **963** L2 [DOI 10.3847/2041-8213/ad21fb](https://doi.org/10.3847/2041-8213/ad21fb)

Sivaramakrishnan, A., Tuthill, P., Lloyd, J. P., et al. The Near Infrared Imager and Slitless Spectrograph for the James Webb Space Telescope. IV. Aperture Masking Interferometry 2023, *PASP*, 135, 015003 [doi: 10.1088/1538-3873/acaebd](https://doi.org/10.1088/1538-3873/acaebd)